Holographic Interferometry Deformation Study of a Printer Type-piece

Abstract: Holographic interferometry with a pulsed ruby laser is used to determine printer type-piece deformation caused by impact of the print hammer. A variety of type-piece designs are examined. Effects of impact velocity and hammer-type-piece alignments are studied. Means of obtaining stress information from the holographic data are considered. Cubic spline methods are used to smooth the holographic data and to obtain continuous first and second derivatives. The stresses calculated from the holographic data agree well with those obtained by other means such as finite element analysis. Some limitations of the holographic technique as well as its advantages are discussed.

Considerable type-piece twisting is observed; this was not expected or known previously. The most significant result is that a type-piece tends to twist when impacted by the hammer at any point other than the exact center. The twist angle is of the same magnitude as the angle of out-of-plane motion of the type. Hence the type may impact the platen on one corner or side edge. Also, the type bends greatly in the necked down region adjacent to the character and does not pivot by a large amount at its bearing point. Twisting motion is propagated from one end of the type to the other.

Introduction

Holographic interferometry is a well established laboratory technique for displacement measurement [1-4]. With a pulsed ruby laser as the light source for the interferometer, dynamic motion measurement can be made [5]. Q-switched pulsed ruby laser hologram interferometry, pioneered by Heflinger, Wuerker and Brooks [6], now enables the researcher to make double-exposure holograms of fast moving objects. This paper discusses an investigation designed to apply established holographic techniques to the analysis of the motion of a printer type-piece impacted by a print hammer. The technique will determine the total motion of the typepiece as a function of time-after-impact; the compiled data will be compared for several type designs, hammer impact velocities, and impact points. The displacements obtained from the holographic technique are known in terms of the wavelength of the laser light used to construct the hologram, and highly accurate displacements can thus be obtained from the resultant hologram fringe systems.

Most important, however, is the determination of the corresponding stresses. Unfortunately, obtaining the stresses from the displacement data requires two numerical differentiations. Therefore, the following comparisons are made:

- 1. The hologram displacements are compared with displacements obtained by the integration of stress solutions; the latter solutions are the result of numerical operations such as finite element analysis [7].
- 2. The stresses of finite element analysis are compared to those obtained by cubic spline fitting techniques [8] applied to the hologram data.

Pulsed laser hologram interferometry does not replace measurements made by other methods, such as strain gauges, but rather complements and enhances the accuracy of the older techniques. In the analysis of a printer type-piece the hologram can show the deformation of the complete front surface of the type-piece at one instant of time. The strain gauge, on the other hand, shows surface strain at one point for all time. Thus, the two techniques are complementary.

Holography is very useful for indicating the location for placing the strain gauge, whereas the strain gauge is beneficial in determining the time at which the hologram should be made. Generally, holography is sensitive to a vector displacement (or deformation) of the object. Strain gauges are usually responsive only to one strain component (unless the gauge is of the Rosette type). Hence, holography may yield a more complete "picture"

of an unknown object deformation. Another advantage of holography is that it does not require any loading of the object nor the installation of sensors. On the other hand, the holographic fringe patterns, which can be quite complicated, must be interpreted to obtain an understanding of the pattern; the technique also suffers from a lack of equipment portability.

Experimental techniques

Holographic analysis of the printer type-piece is performed using the interferometer of Fig. 1. The light source is a ruby laser having a two-trigger Pockels cell switch within the cavity. This Q-switch enables the generation of two, 20-ns laser pulses within the same flash-lamp cycle. There is sufficient energy in two laser pulses to holographically expose the photographic emulsion (AGFA-Gevaert 10E75).* Hence, the two exposures of a double-exposure hologram are made during the single flash-lamp (laser pump) cycle, with a timing between pulses adjustable from 100 to 1000 μ s. Because of the high irradiances, most optical components in Fig. 1 are of the low-loss, multicoat dielectric type.

The ruby laser (a Korad, model K1DQH)† operates in a TEM₀₀ mode and has a coherence length of 100 cm. This long coherence length does not require precisely equal optical paths in the two arms (reference and signal) of the holographic interferometer. However, optical paths are matched to within a few centimeters. The energy per pulse is about 20×10^{-3} Joules. The laser pulse is 20 ns in width at the half-power point, and the operating wavelength is 649.3 nm. Illumination of the typepiece was accomplished by focusing a collimated wave with a long focal length cylindrical lens and locating the type-piece near the focal plane. With this method, a considerable amount of light can illuminate a long thin object such as the type-piece without illuminating the surrounding area. The irradiance at the hologram plane due to the object wave is therefore light diffusely reflected by the object in motion, and not by a large surrounding area. Proper selection of the beam splitter and a distributed-type, neutral density attenuation filter in the reference wave adjusts the irradiance of the reference and object waves so that the irradiance of the reference wave is about twice that of the object wave. The object wave irradiance is determined for a polarization equal to that of the reference wave. The ruby laser radiation (laser pulse) is vertically polarized (S-polarization with respect to the optics used); however, the diffuse object tends to emit or reflect a partially unpolarized wave. The hologram plate normal (perpendicular) is set to bisect the average angle between the object and reference

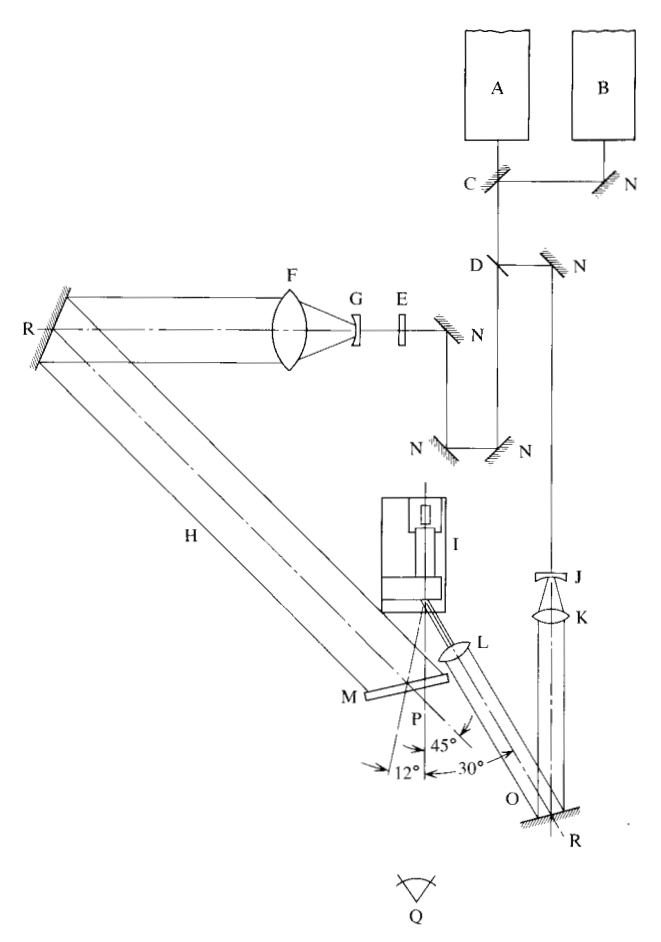


Figure 1 Holographic interferometer. A, helium neon alignment laser; B, Korad K1QDH ruby laser; C, removable mirror; D, beamsplitter, (92% reflected, 8% transmitted); E, attenuator; F, collimator; G, spherical lens; H, reference wave; I, object; J, spherical lens; K, collimator; L, 150 mm cylindrical lens; M, emulsion; N, 100% reflective dielectric mirrors; O, illuminating wave; P, viewing wave(s); Q, observer; R, aluminum mirrors.

waves. This minimizes any effects of emulsion shrinkage due to processing.

The value of a fringe in diffuse interferometric holograms depends not only on the wavelength, but also on the illuminating and viewing geometry. The change in phase $\Delta \phi$ of the wavefront due to a vector displacement d of the object, where the object illumination and viewing directions are \hat{i} and \hat{r} respectively, is

$$\Delta \phi = \frac{2\pi}{\lambda} \, \mathbf{d} \cdot (\hat{\imath} + \hat{r}) \,. \tag{1}$$

This relationship, as well as the underlying principles of fringe formation and localization in hologram interferometry, is discussed in the works of Tsuruta [9] et al., Stetson [3,10], Molin and Stetson [11], Froehly [12] et al., Sollid [13], Welford [14] and Wilson [15,16].

^{*}Manufactured by AGFA-Gevaert, Inc., Teterboro, New Jersey.

[†]Manufactured by the Korad Dept., Union Carbide Corp., Santa Monica, California.

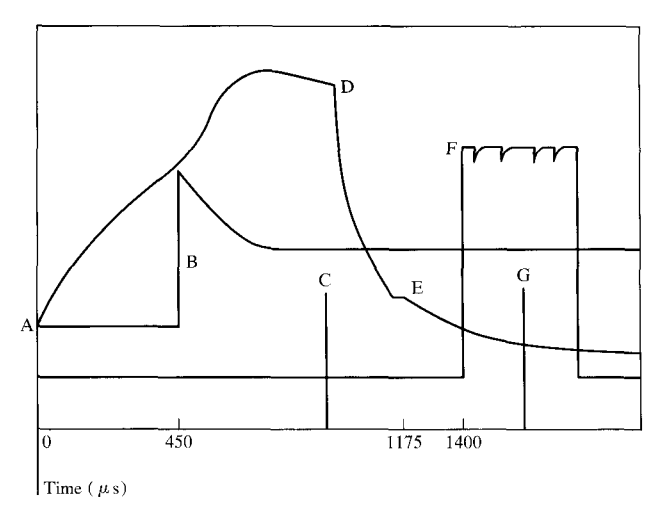
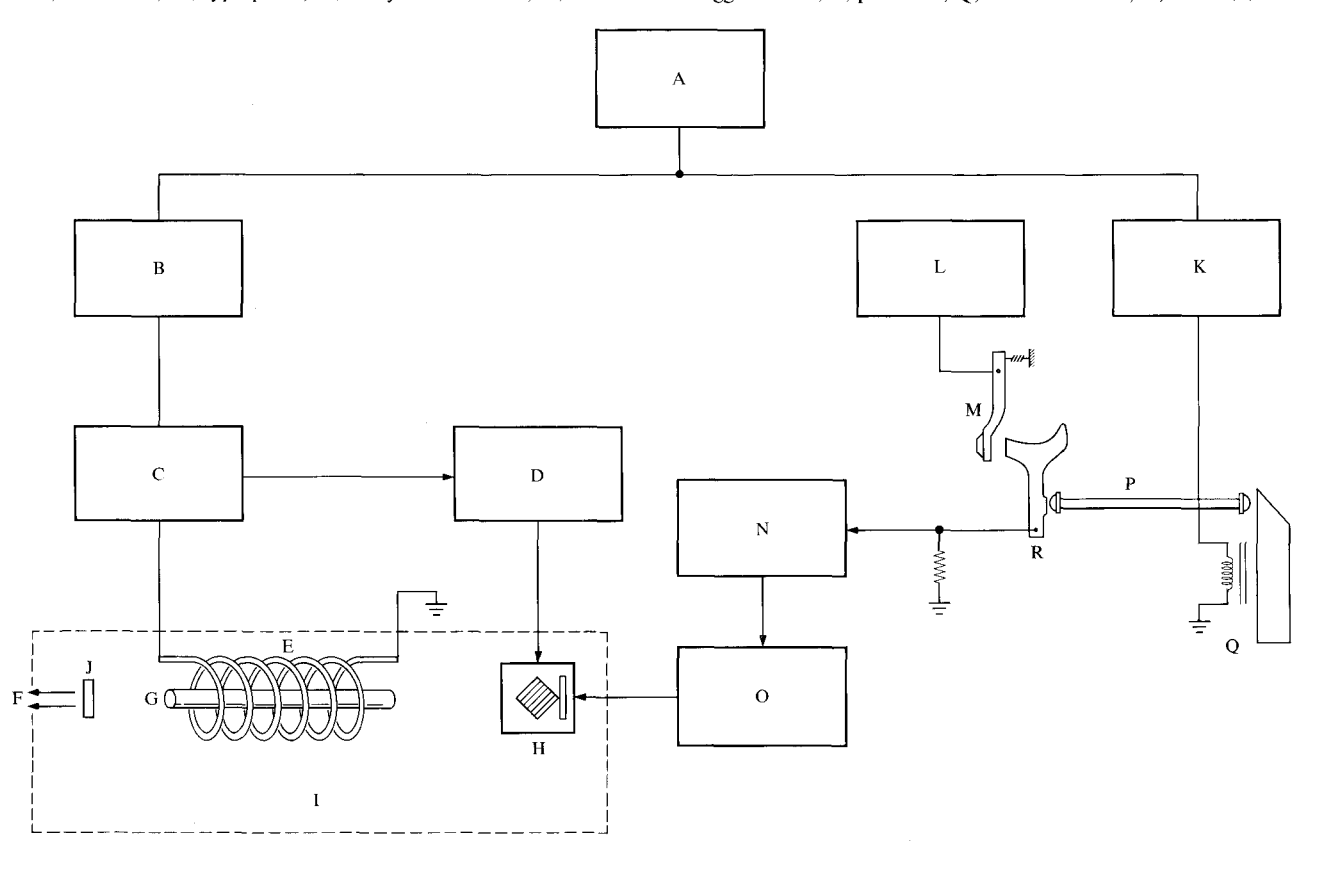


Figure 2 Driver coil current and laser timing sequence. A, start of driver coil current; B, start of flash lamp cycle; C, first laser pulse; D, coil current waveform; E, seal time of armature; F, contact of hammer and type; G, firing of the second laser pulse.

For the type-piece it is found that the type moves principally in a direction parallel to the normal of the actual type face. Transverse motions are restricted by the type mounting and are not likely. For the described illuminating and viewing geometry, the holographic interferometer is not highly sensitive to transverse motions. For the angles of illumination and view, 30° and 12° , respectively, the value of d necessary to change $\Delta \phi$ by 2π radians is determined from Eq. (1) to be 377 nm (14.8 μ in.). This is the displacement necessary to cause one fringe (bright to bright or dark to dark) to occur.

The technique for recording the double-exposure holograms of the type-piece involves making the first exposure sometime after the hammer driver coil has been actuated and before impact of the hammer and type-piece (Fig. 2). Thus the first exposure is made of the type-piece at rest. The second exposure is made at some selected time after impact: for example, $10 \, \mu s$. Time of hammer/type-piece impact is determined by sensing the first electrical contact of these two bodies. This contact triggers a pulse generator whose delay is adjusted to obtain the correct firing time for the second laser pulse.

Figure 3 Block electrical diagram. A, manual start; B, flash lamp delay; C, flash lamp capacitor and trigger circuit; D, Pockels cell trigger No. 1; E, flash lamp; F, laser pulse; G, ruby rod; H, Pockels cell and 100% mirror; I, ruby laser; J, etalon; K, hammer driver circuit; L, +30 V; M, type-piece; N, delay after contact; O, Pockels cell trigger No. 2; P, push rod; Q, hammer driver; R, hammer.



The delay is measured with a counter. Figure 3 shows a block diagram of the electronics, Fig. 4 shows the model used, and Fig. 5 indicates an outline of the type.

The velocity of the hammer is dependent on several different parameters. With these parameters set correctly, the hammer free-flight time is about 1400 μ s. This results in a hammer velocity of about 4.8 m/s (190 in./s).

To construct a double-exposure hologram with good fringe visibility, it is necessary to have two ruby laser pulses with nearly the same energy. This is done by carefully choosing the time of the first pulse with respect to the beginning of the flashlamp cycle and the time delay between the pulses. The procedure is one of trial and error.

The holograms in this study are recorded on 4×5 in. AGFA-Gevaert 10E75 emulsion developed in Kodak D-19* for 6 min. at 68°F, stopped in Kodak stop for 30 s and fixed in Kodak rapid fixer for 4 min., washed in water at 72°F for 30 min., and air-dried. The sensitivity of the emulsion to pulsed ruby radiation is approximately 50 to 100 erg/cm². Note that the holograms are recorded with a collimated reference wave.

To photograph the hologram, the plate is placed in a reconstructing wave that traverses the emulsion in a direction opposite to that of the original reference wave. The reconstructing wave is produced by a helium-neon gas laser. The wavelength of this laser is not equal to that of the ruby laser. Nevertheless, the value of **d** remains unchanged; thus, one fringe corresponds to a displacement equal to **d** or 377 nm. The result is a real image, nearly free of aberrations, and this image is recorded using a view camera.

Although the hologram of the type-piece presents a reconstructed three-dimensional image, the spatial depth of the type-piece is lost in the two-dimensional photo. This presents a problem, because the fringes formed are not necessarily localized exactly on the object, and the object is not in one plane. Some choice as to where to focus the recording camera must therefore be made, and the fringes of greatest importance have been selected to be the point of best focus. Unfortunately, because of speckle effects, the camera aperture cannot be made arbitrarily small to increase depth of field.

Experimental results

The experimental results shown in Figs. 6 through 13 are photographs taken of the holograms. Figures 6 and 7 depict a J-type design for normal hammer impact alignment [Fig. 14(a)] with the indicated impact velocities and delays after hammer impact $(T_{\rm d})$. The fringes found on the hologram images of the type-piece are due to a vector displacement of the type. The displacement is the

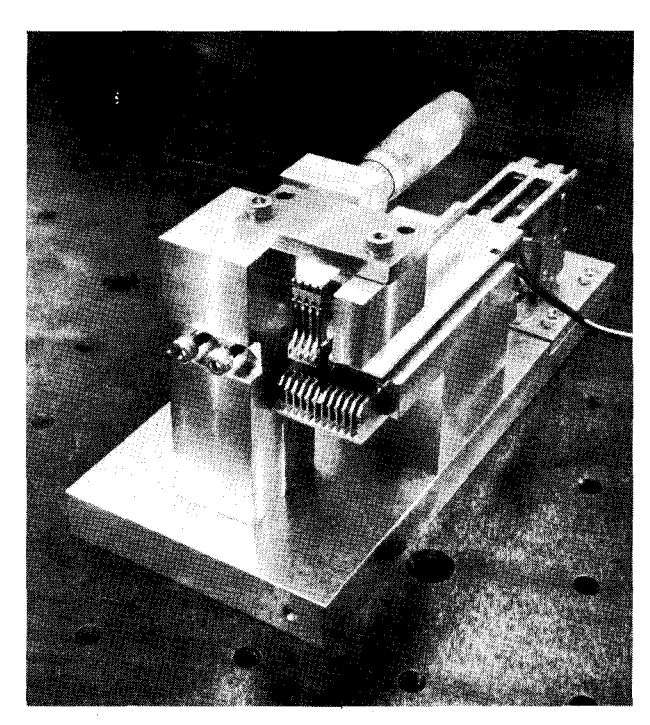
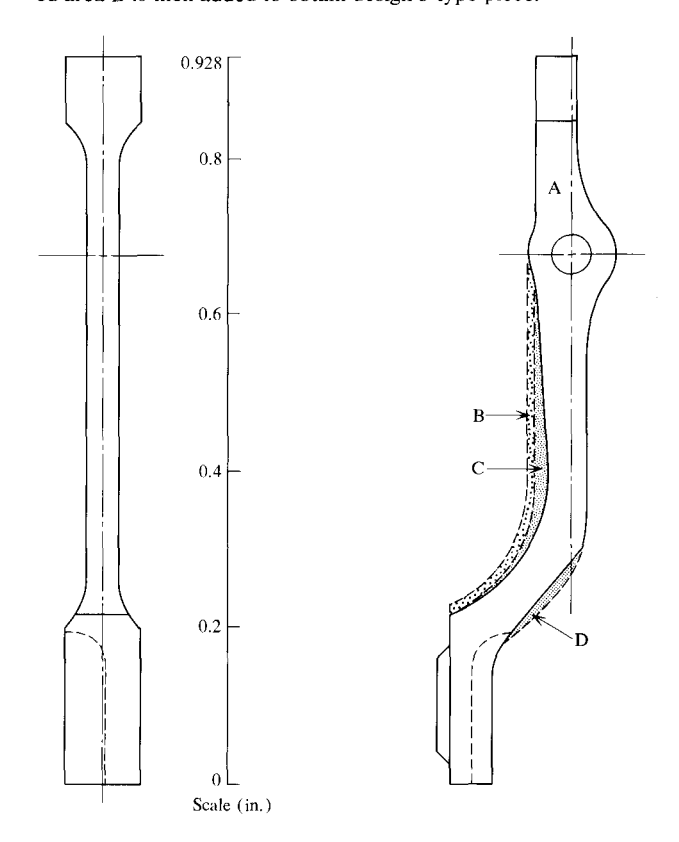


Figure 4 Test model.

Figure 5 Type-piece outlines; the unshaded area within the solid lines shows the profile of design 1 type-piece; the shaded area C is added to design 1 to obtain design 2 type-piece; shaded area B is then added to obtain design 3 type-piece.



^{*}Manufactured by Eastman Kodak Corp., Rochester, N.Y.

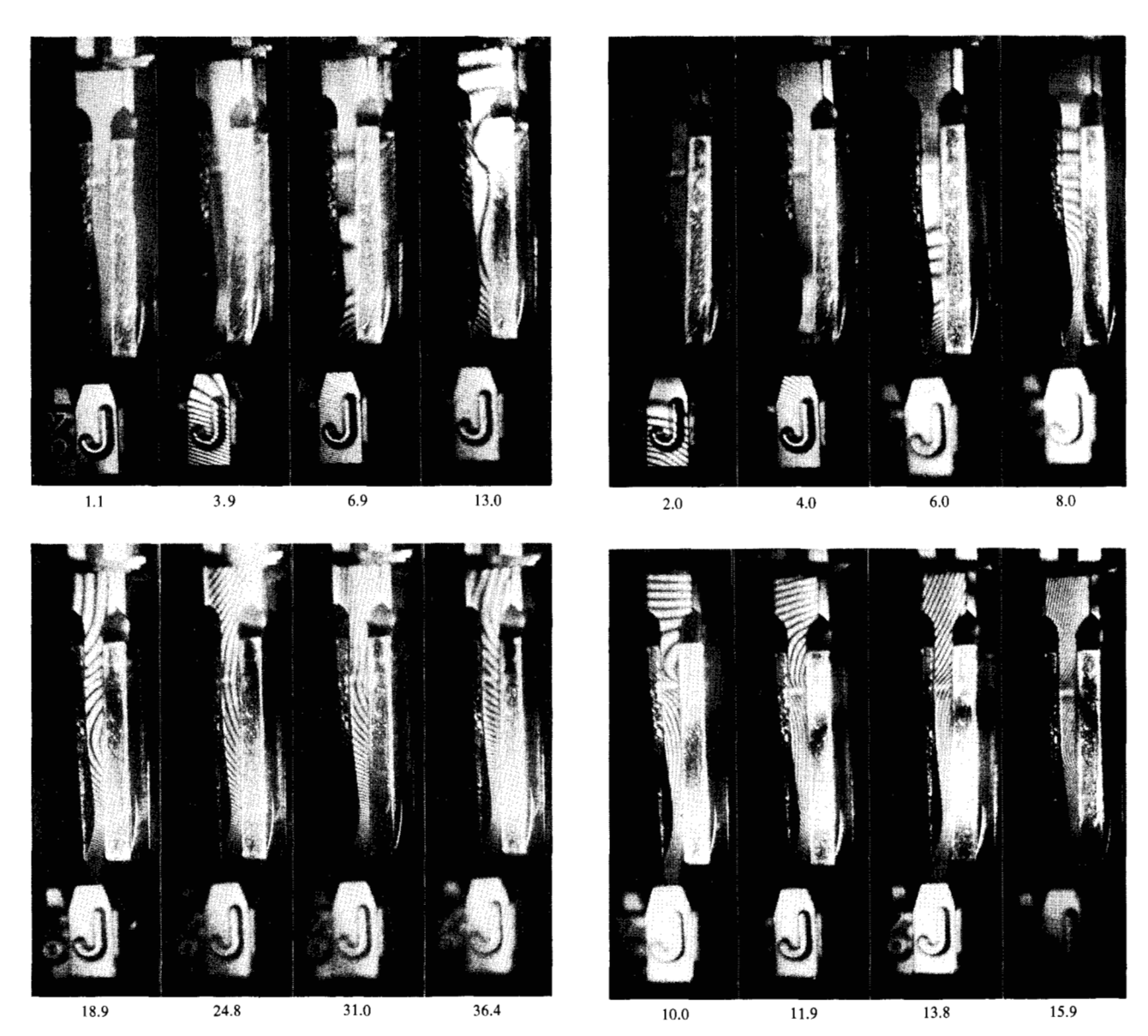


Figure 6 J type-piece design 1 at 70 in./s, normal alignment. Numbers are $T_{\rm d}$ in microseconds.

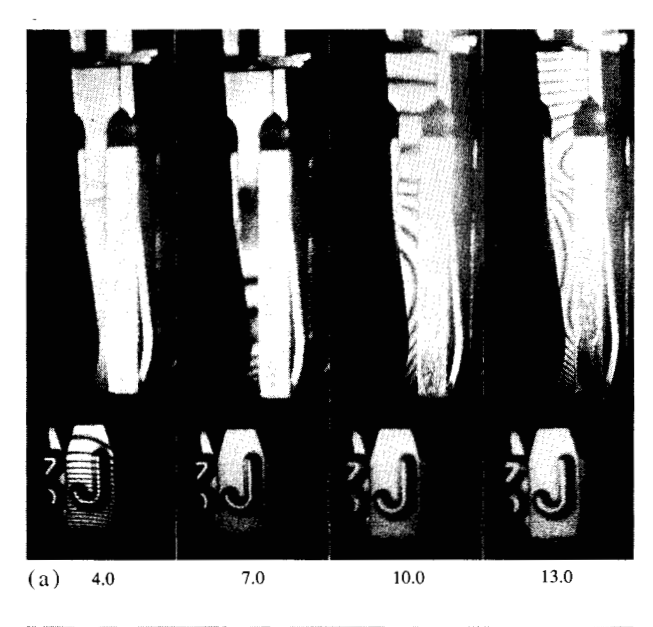
Figure 7 J type-piece, design 1 at 170 in./s, normal alignment. Numbers are T_d in microseconds.

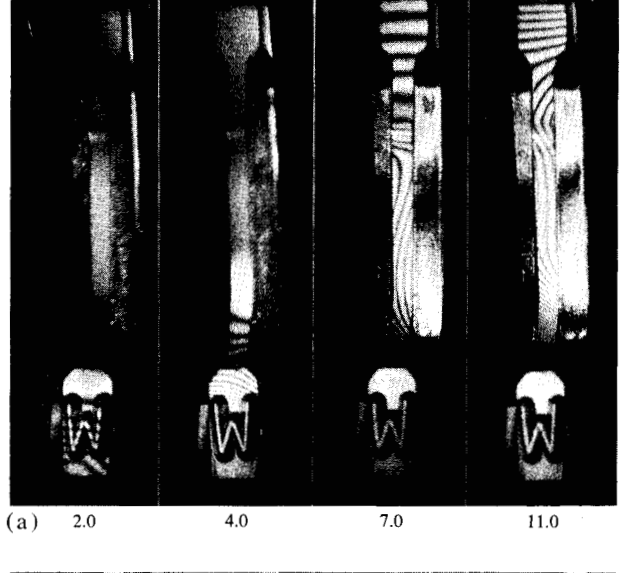
change in type-piece form from its rest-position shape to its dynamic shape. Each fringe (bright-to-bright) found here is due to approximately 15 microinches of displacement. Fringes that run perpendicular to the long axis of the type-piece are due to motion about the pivot axis of the type-piece. Fringes that run parallel to the long axis of the type are due to motion about the longitudinal axis (this is most probably rotation or torsion-twisting of the type). Figures 8(a) and 8(b) are photographs of the same type-piece showing the effects of misaligning the hammer from the normal by the amount indicated. For these Figures the hammer is misaligned from the normal condition with the positive direction being such that more of the hammer face is in contact with the flat back of the

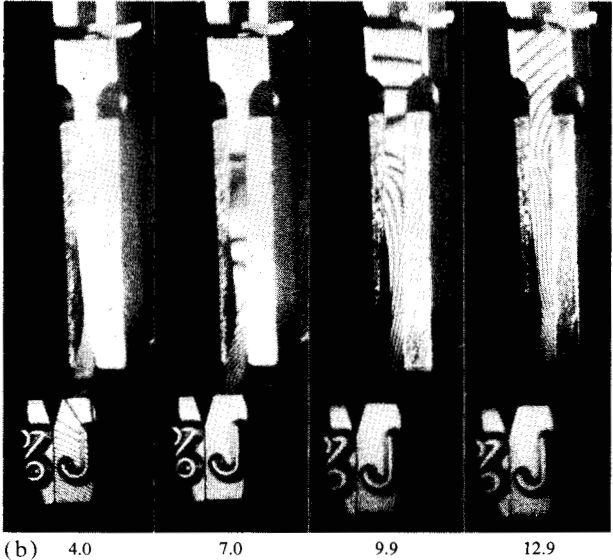
type-piece. A positive misalignment means greater misalignment. Thus, the positive alignment tends to cause greater twisting of the type, evidenced by the greater number of axial fringes in Fig. 8(b), because the point of impact is not at the center of mass.

Figures 9 through 11 show the displacement of a W type-piece for three different type designs. Although the outlines appear the same, the thicknesses (depths) of the type-pieces are different (see Fig. 5). Each figure is of a different type design.

In Fig. 12, normal hammer-type alignment is used, but the hammer is a special one; the face of the hammer is ground so that only a small area in the center will contact the type-piece [see Fig. 14(b)]. In Figs. 12(a) and







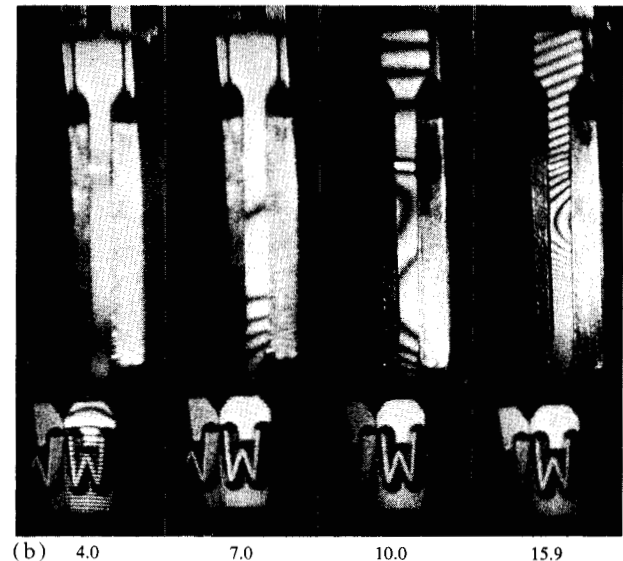


Figure 8 J type-piece, design 1 at 118 in./s, misaligned (a) -0.008 in.; (b) +0.008 in. Numbers are T_d in microseconds.

Figure 9 W type-piece, normal alignment, design 2 at (a) 170 in./s; (b) 120 in./s. Numbers are T_d in microseconds.

12(b) the effects of using the raised hammer to impact the asymmetrical-backed W type-piece are seen. Figure 12(a) shows the displacement with the raised hammer aligned as shown in Fig. 14(b), whereas Fig. 12(b) has the raised hammer misaligned by 0.010 in. in the positive direction.

Figure 13 shows the static displacement of the typepiece when the hammer is brought into contact with the type-piece and then moved forward by means of a microinch micrometer screw.

The photographs of Figs. 6 through 13 are examined with a measuring microscope, and the physical position of each fringe is located. Profiles of the J-type (impacted at 170 in./s) shape are shown first in summary in Fig. 15

and then a few sample detail profiles are shown in Fig. 16.

Numerical techniques and results

Obtaining stress values from the holographic displacement data is done by using spline techniques. The spline techniques are used because they seem to be the best method available for obtaining continuous first and second derivatives. Cubic spline functions are used. In the spline smoothing, the displacement data are smoothed, and the derivative of the displacement is determined. Next, the derivative is spline-smoothed, and its derivative computed. This is the second derivative of the displacement.

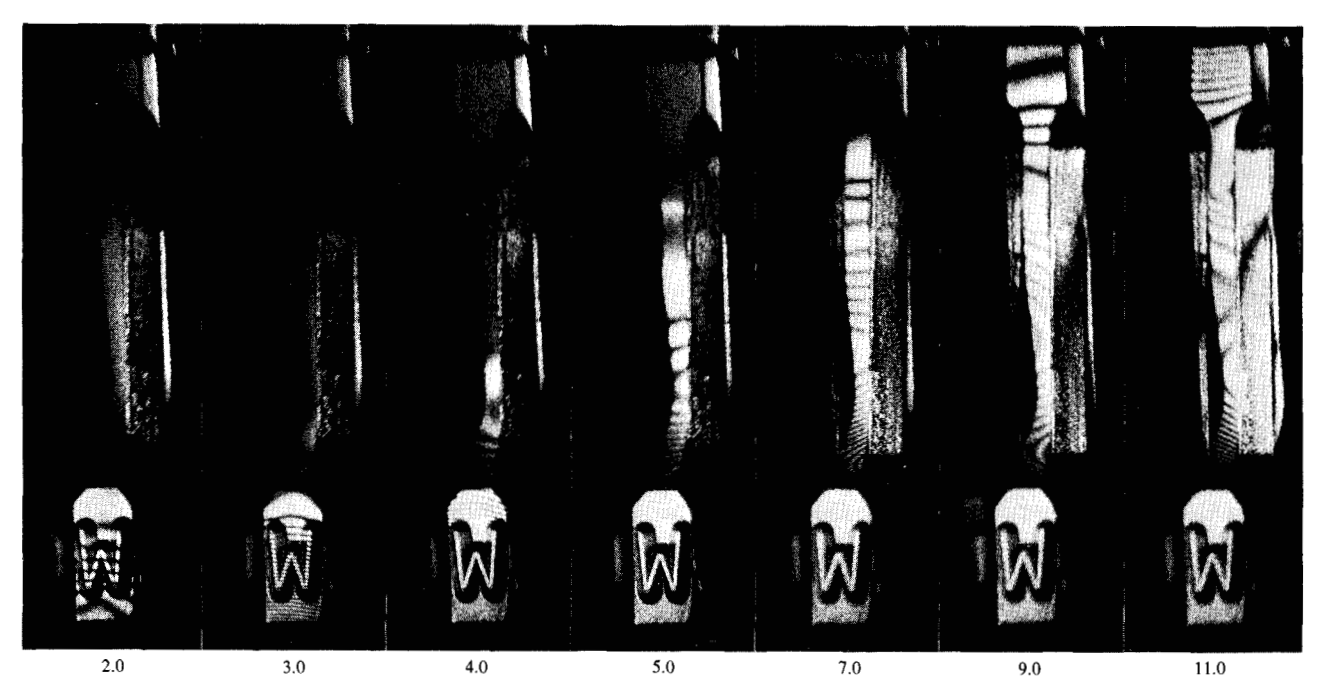


Figure 10 W type-piece, design 1 at 170 in./s, normal alignment. Numbers are T_d in microseconds.

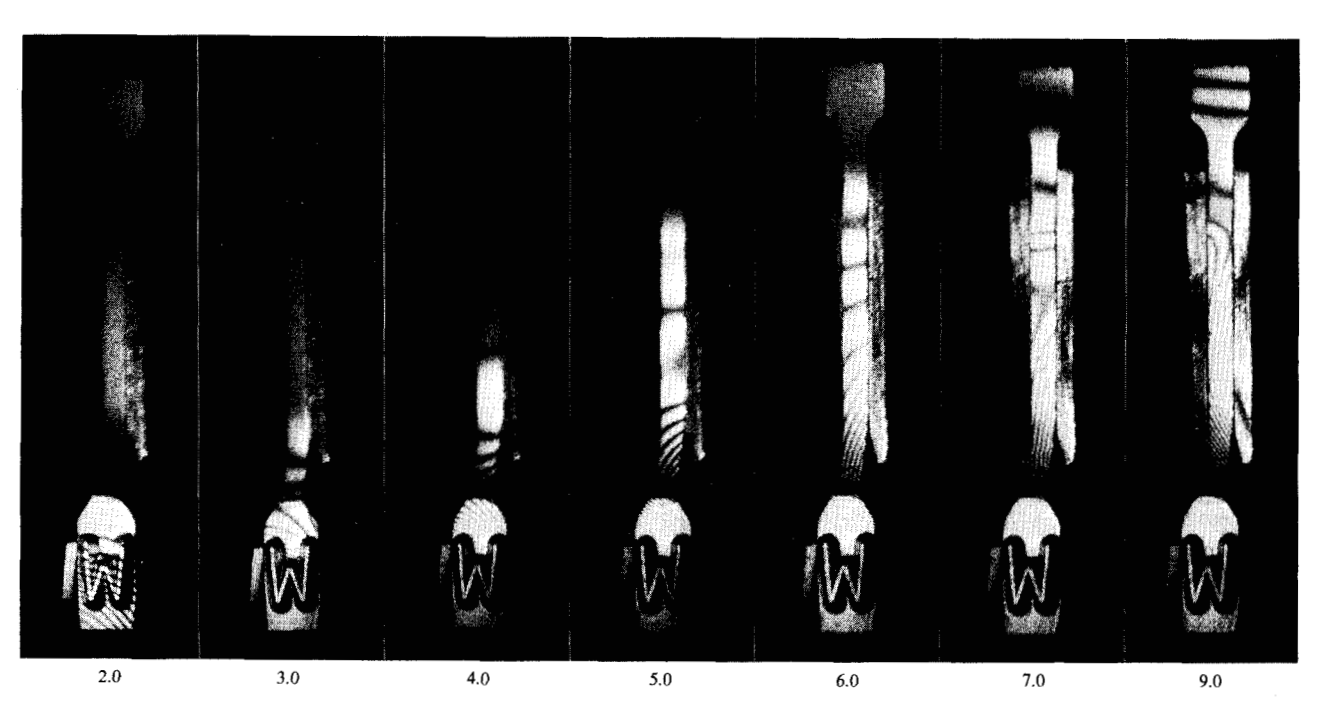
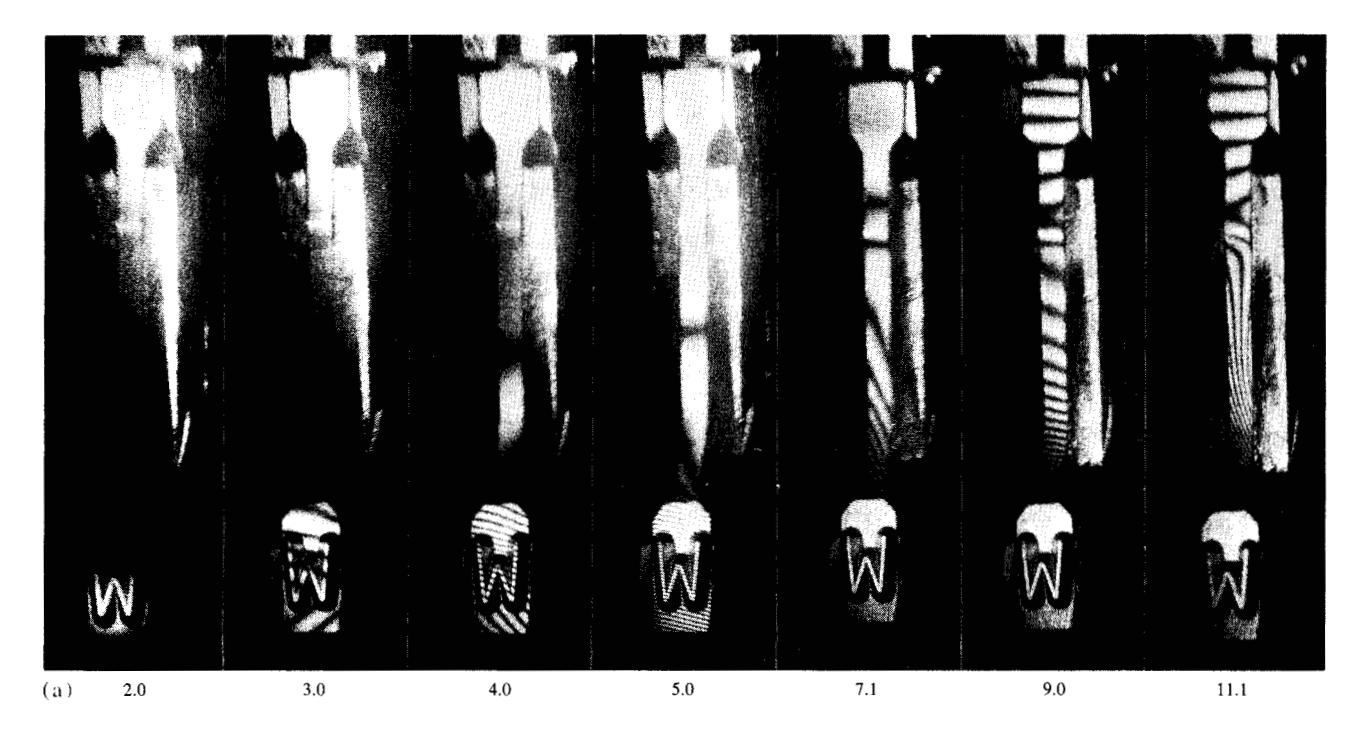


Figure 11 W type-piece, design 3 at 170 in./s, normal alignment. Numbers are T_d in microseconds.

The second derivative of a sample displacement curve is shown in Fig. 17. The ordinate scale is a second derivative in μ in./in.², and the abscissa is the position on the type in inches. Because of the material constants and size of type-piece, the stress has nearly the same numerical value as the scale (ordinate) of the second deriva-

tives. Thus, the ordinate can be thought of as stress in psi or second derivative in μ in./in².

In Fig. 18(a) the second derivative distribution is shown for a J-type design at 55 in./s and 22 μ s after impact. For comparison, Fig. 18(b) shows the second derivative at 20, 22, and 24 μ s, as determined by Lee



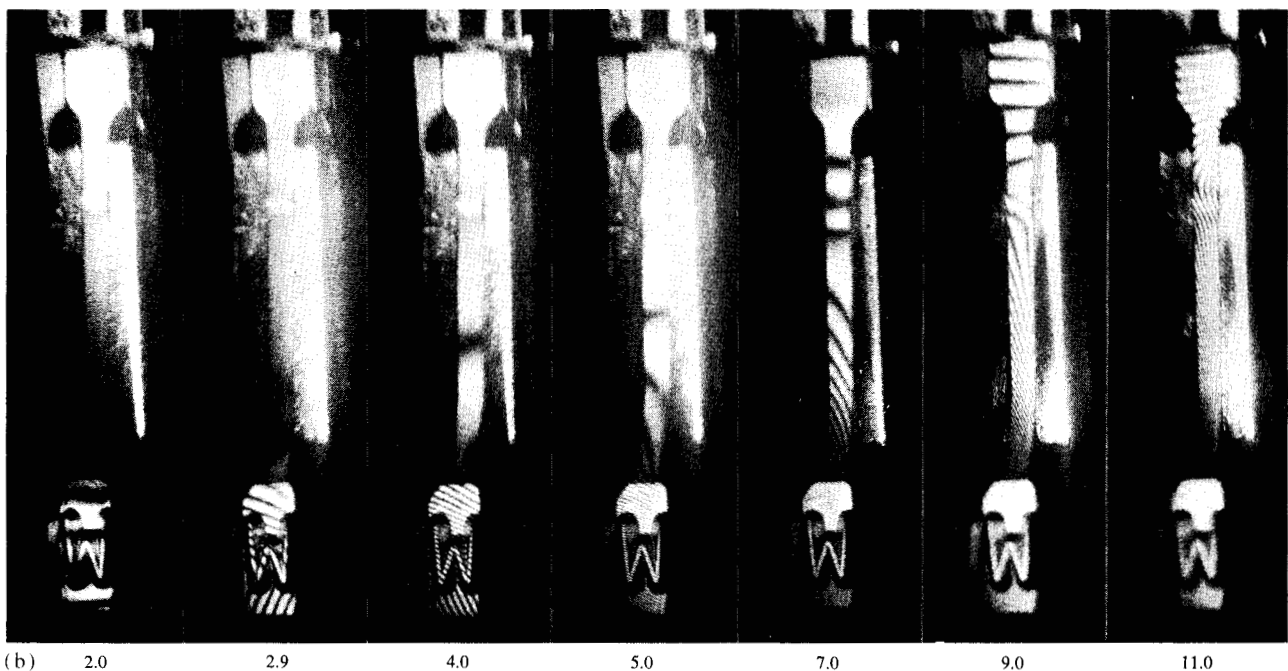


Figure 12 W type-piece, design 1 at 170 in./s, special hammer. (a) Best possible impact condition; (b) misaligned +0.10 in. Numbers are T_d in microseconds.

[7] using finite element methods for the same typepiece and impact velocity. The agreement at a time of $22 \mu s$ for the location and the maximum of the second derivative level is quite good. Shown in Fig. 19 are the second derivatives of displacement for the three different type designs of Fig. 5. It is clear that the derivative maximum decreases as the thickness of the type increases. Least-square fitting of polynomials was examined; it was found that, while extremely good fits to the displacement data could be obtained, little confidence could be given to the second derivative of the polynomial fit. For example, good fourth through tenth order polynomial fits were obtained for the data used to generate Fig. 18(a). However, only sixth- and seventh-order poly-

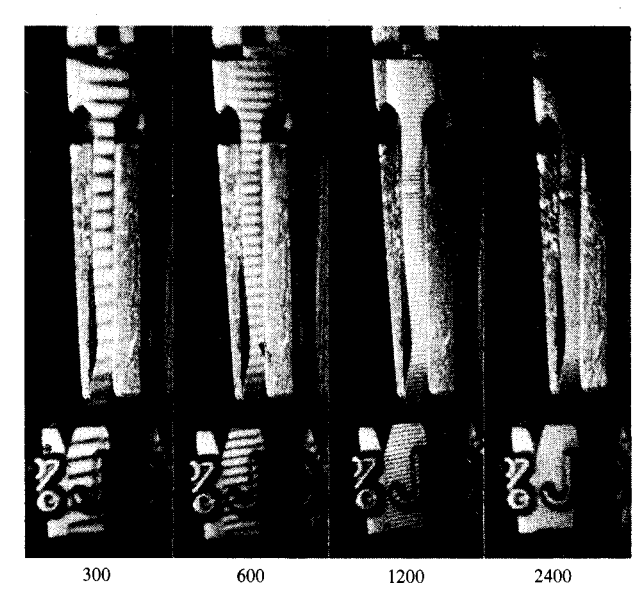
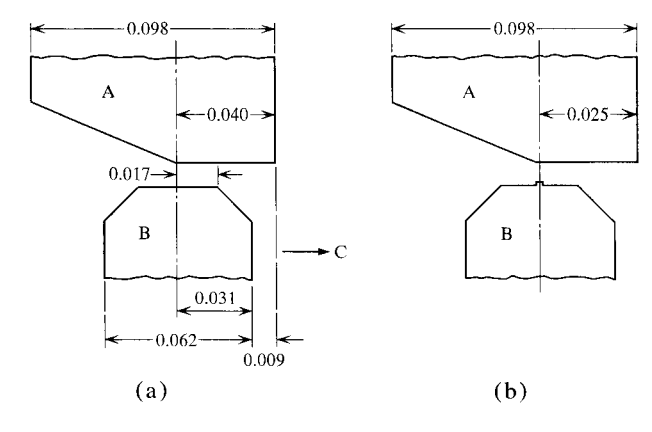


Figure 13 Static displacement of type, 300, 600, 1200, 2400 μ in.

Figure 14 (a) Hammer type-piece alignment (numerical values in inches): A, type; B, hammer; C, direction of positive misalignment. (b) Specially ground hammer type-piece alignment (values in inches): A, type; B, raised hammer.



nomials yielded second derivatives resembling the curve of Fig. 18(a).

General discussion and conclusions

The hologram fringe patterns reveal that it is very difficult to obtain a deflection of the type-piece that does not contain considerable rotation of the type about its long axis. This is due to the asymmetrical design of the type rear-face and point of hammer impact. The effect of the rotation on print quality is not the subject of this investigation. It is evident, however, that the type will twist more often than not, and that the twist is a dynamic situation. Conditions of no twist were found to be possible by carefully adjusting the point of impact of a special

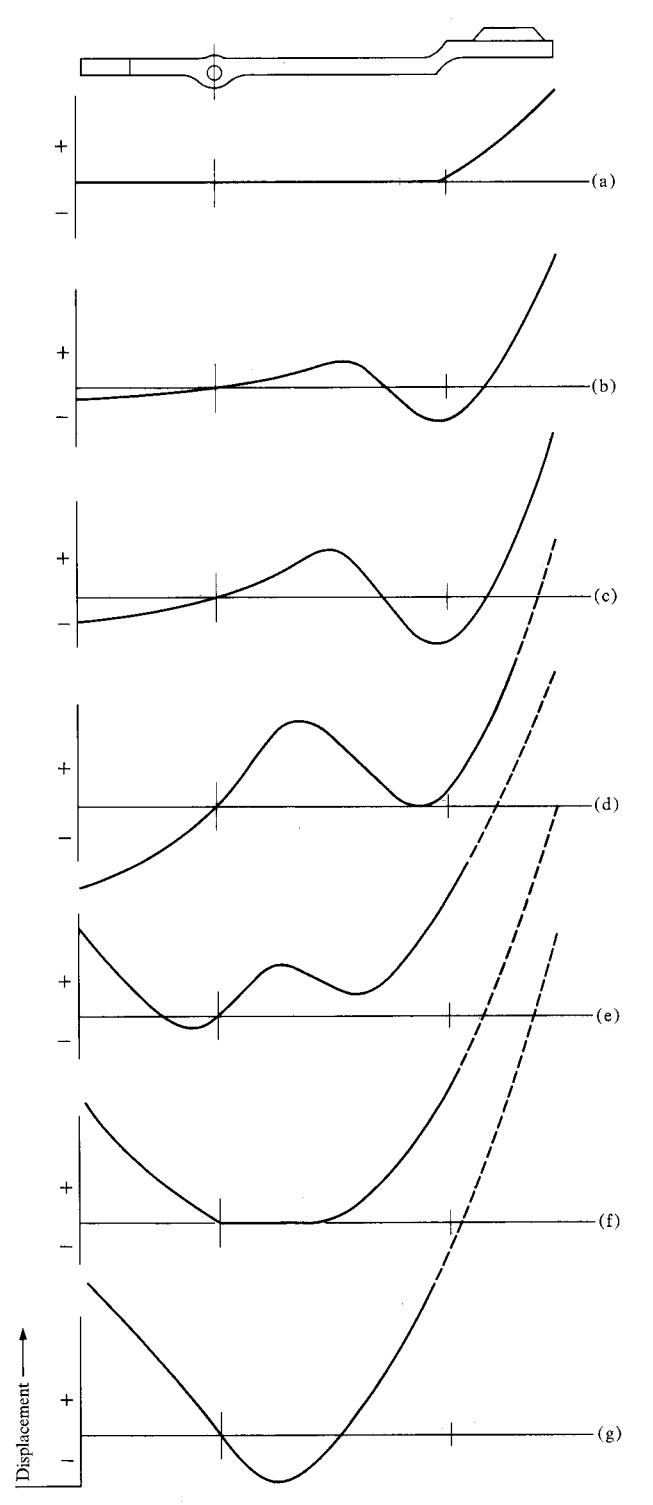


Figure 15 Displacement envelopes at indicated times for J type, design 1, impacted at 170 in./s; $T_d = (a) 3.0$, (b) 5.0, (c) 7.0, (d) 9.0, (e) 11.0, (f) 12.9, and (g) 15.9 μ s.

hammer on a symmetrical type. We shall arbitrarily define the y-axis to lie along the type, the z-axis to lie normal to the type face, and the x-axis to be perpendicular to the y-axis and in the plane of the type. Moreover, the

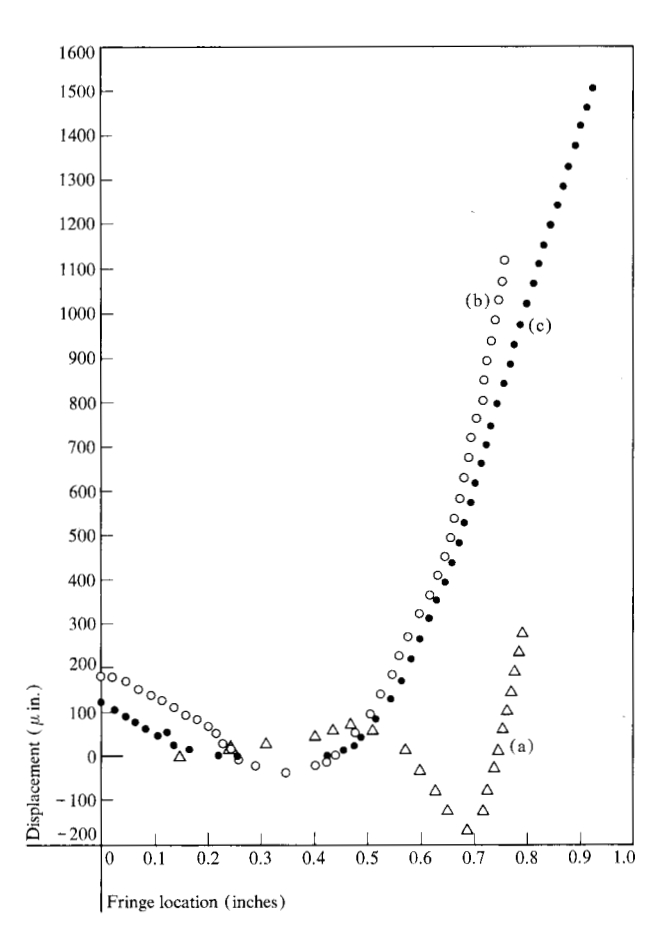
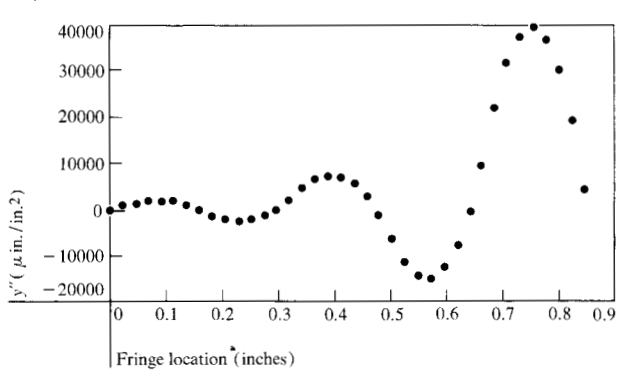


Figure 16 Displacement of J type, design 1, at (a) 6, (b) 13.8 and (c) 21.0 μ s after impact at 170 in./s.

Figure 17 Second derivative at 4 μ s for J type impacted at 170 in./s.



angle of twist about the y-axis in the neck region is about equal to the angle of the out-of-plane motion in that same region. This is easily observed by noting the angle the fringes make with respect to the y-axis. For example, a 45° diagonal fringe indicates constant z displacements (out of the plane of the page) for equal x and y positions.

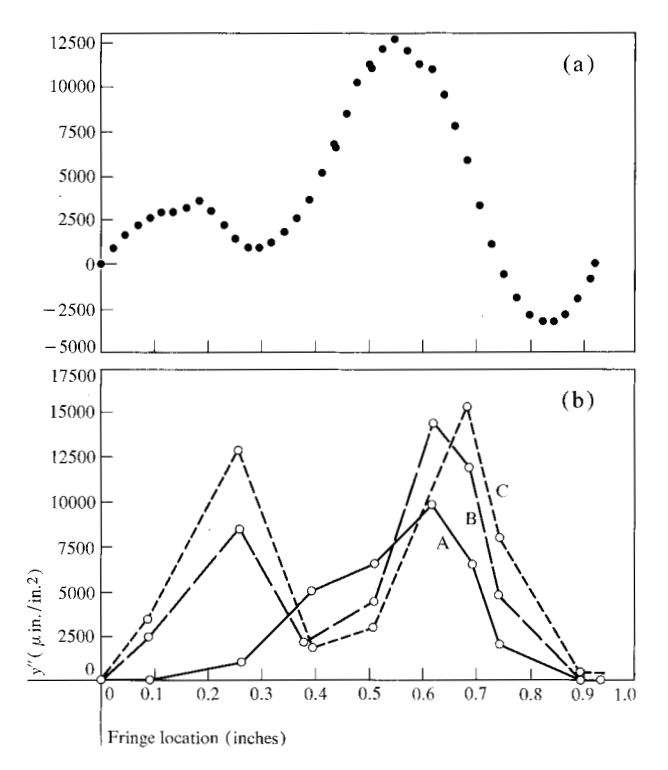
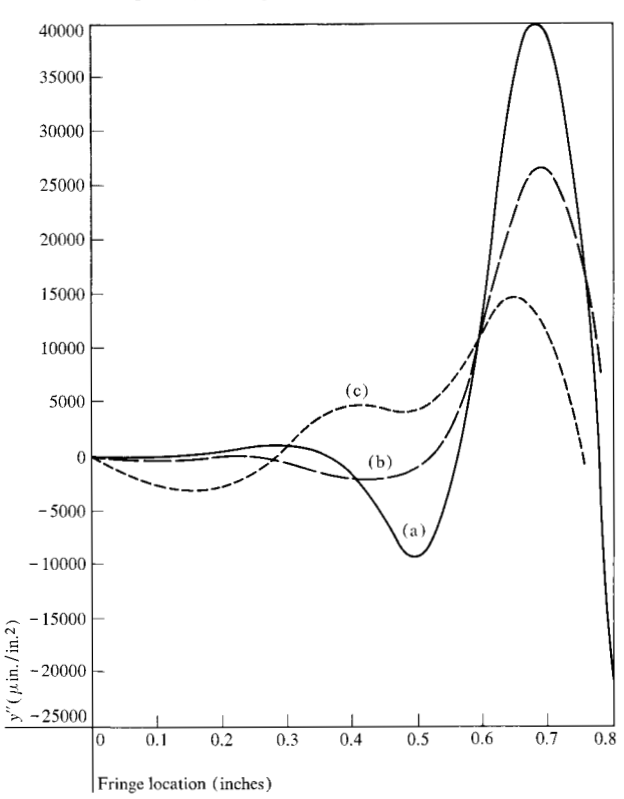


Figure 18 (a) Second derivative at 22 μ s for J type impacted at 170 in./s. (b) Lee finite element result: A, 20; B, 22; C, 24 μ s.

Figure 19 Second derivative for W type at $10 \mu s$ and 120 in./s: (a) design 1; (b) design 2; (c) design 3.



See, for example, Fig. 6 at $6.9 \mu s$ where the fringes are inclined about 10° .

The number of fringes present in the transverse (x) direction is insufficient to accurately measure the stress due to twisting; however, because the axial (y) component of the fringes changes along the type and with time (see Fig. 7 and notice the end opposite the type character for times 10 through 15.9 μ s), it is believed that observed rotations are due at least in part to torsion and not to a poorly fitted bearing. When the type is deflected almost in a static condition (i.e., with a micrometer on the hammer), then no twisting is observed (see Fig. 13). The best (least rotation of shank) deflections were those obtained in Fig. 8(b).

Because of the large number of fringes present at the time of impact with the paper and platen, it was not possible to determine the type shape. However, it is apparent from the available data that if the free end of the type-piece starts with some twist, then it continues to twist at least until the time at which the fringe visibility goes to zero and probably until contact with the platen. Hence, by the time the type-piece reaches the paper, one side of the character may lead or lag the other by as much as 0.5×10^{-3} in. from a total travel of 2 to 3 $\times 10^{-3}$ in. For close type-platen distances, this could result in poor printing of characters such as an O. Other characters might print poorly depending upon which way the type was twisting at the time of impact. For large type-platen distances (10×10^{-3} in.), the twisting may be even more severe and result in as much as 2×10^{-3} in. of lead or lag on one side. This is too large a distance to be easily measured by holography, but can be measured by other techniques. Much of this tilting type displacement stems not from warpage of the character section of the type, but rather from twisting in the neck region.

The magnitude of the stresses calculated by the spline smoothing methods seem reasonable. Of greatest significance will be the point at which the stress is a maximum so that one may then place a strain gauge at that point. Unfortunately, it appears that one point has maximum stress for a specific time, but at another time the maximum is at a different physical point. Holography gives some indication as to the location of the stress maximum at one specific time. It does not tell whether that time is the time of maximum stress. This situation is perplexing; however, strain gauges tell only what the maximum stress is at one point. For a different point and time, the stress will reach another maximum. Thus, neither technique is complete.

There is one limitation of the holographic method which is reached in this analysis: To obtain a hologram, the relative phase of the reference and object wavefronts or their combination should not change by more than

 $\pi/4$ radians during the exposure. The exposure time is very short, being of the order of 20×10^{-9} seconds, but because the maximum velocity of the type is large (200 in./s), the wavefront from the type-piece violates the $\pi/4$ radians stability criterion for velocities greater than about 100 in./s. Therefore, holograms can be made of the type-piece only when the type velocity is less than 100 in./s. Consequently, holograms are made at normal machine impact velocities, but for a limited time after impact and then at lower impact velocities, for longer times. For the higher impact velocities, certain fastmoving segments of the type do not reconstruct useful images (no fringes). Lower-velocity regions continue to produce useful images. Also, for long delay times between exposures (10 to 20 μ s), the type movement may generate too many fringes to be resolved (too high a fringe frequency) because of the large displacements involved and the decrease in fringe visibility with increased displacement. For example, at a type velocity of 200 in./s, 400 fringes would be generated for a delay of $10 \,\mu s$.

Acknowledgments

The authors thank G. Wylie for supplying the hardware used in this study and for his guidance during the project. Special thanks go to S. Tsao and B. Lee for their assistance with the analysis of the holographic data, and to R. D. Owczarzak for his assistance with the manuscript.

References

- K. A. Stetson and R. L. Powell, J. Opt. Soc. Am. 56, 1161 (1966).
- K. A. Haines and B. P. Hilderbrand, Appl. Opt. 5, 595 (1966).
- 3. K. A. Stetson, Optik 29, 386 (1969).
- 4. H. M. Smith, *Principles of Holography*, Wylie-Interscience. New York 1969.
- 5. F. P. Burns, IEEE Spectrum 4, 115 (1967).
- L. O. Heflinger, R. F. Wuerker and R. E. Brooks, "Holographic Interferometry", J. Appl. Phys. 37, 642 (1966).
- Private communication with C. H. Lee of our laboratory who has done a finite element analysis of the same typepiece.
- 8. The technique and programs for the cubic spline analysis were supplied by S. Tsao of our laboratory in a private communication.
- 9. T. Tsuruta et al, Optica Acta 723 (1969).
- 10. K. A. Stetson, Optik 31, 576 (1970).
- 11. N-E. Molin and K. A. Stetson, Optik 31, 3 (1970).
- 12. G. Froehly et al, Optica Acta 16, 343 (1969).
- 13. J. E. Sollid, Appl. Opt. 8, 1587 (1969).
- 14. W. T. Welford, Opt. Comm. 1, 123 (1969).
- 15. A. D. Wilson, Appl. Opt. 9, 2093 (1970).
- 16. A. D. Wilson, Appl. Opt. 10, 908 (1971).

Received July 16, 1971

The authors are located at the IBM Systems Development Division Laboratory, Endicott, New York 13760.